Stellar Collisions and the Interior Structure of Blue Stragglers

James C. Lombardi, Jr. and Jessica Sawyer Warren[1]

Department of Physics and Astronomy, Vassar College, 124 Raymond Avenue, Poughkeepsie, NY 12604-0754

Frederic A. Rasio[2]

Department of Physics, MIT 6-201, Cambridge, MA 02139

Alison Sills[3]

Department of Physics and Astronomy, Leicester University, England, LE1 7RH

and

Aaron R. Warren[1]

Department of Physics and Astronomy, Vassar College, 124 Raymond Avenue, Poughkeepsie, NY 12604-0754

ABSTRACT

[1]Present address: Dept. of Physics and Astronomy, Rutgers Univ., Piscataway, NJ 08854

[2]Present address: Dept. of Physics and Astronomy, Northwestern Univ., Evanston, IL 60208

[3]Dept. of Physics and Astronomy, McMaster Univ., Hamilton, Ontario, L8S 4M1, Canada

Collisions of main sequence stars occur frequently in dense star clusters. In open and globular clusters, these collisions produce merger remnants that may be observed as blue stragglers. Detailed theoretical models of this process require lengthy hydrodynamic computations in three dimensions. However, a less computationally expensive approach, which we present here, is to approximate the merger process (including shock heating, hydrodynamic mixing, mass ejection, and angular momentum transfer) with simple algorithms based on conservation laws and a basic qualitative understanding of the hydrodynamics. These algorithms have been fine tuned through comparisons with the results of our previous hydrodynamic simulations. We find that the thermodynamic and chemical composition profiles of our simple models agree very well with those from recent SPH (smoothed particle hydrodynamics) calculations of stellar collisions, and the subsequent stellar evolution of our simple models also matches closely that of the more accurate hydrodynamic models. Our algorithms have been implemented in an easy to use software package, which we are making publicly available (see http://vassun.vassar.edu/∼lombardi/mmas/). This software could be used in combination with realistic dynamical simulations of star clusters that must take into account stellar collisions.

Subject headings: celestial mechanics, stellar dynamics – globular clusters: general – hydrodynamics – stars: blue stragglers – stars: evolution – stars: interiors – stars: rotation

1. Introduction and Motivation

Blue stragglers are stars that appear along an extension of the main sequence (MS), beyond the turnoff point in the color-magnitude diagram (CMD) of a cluster. All observations suggest that blue stragglers are indeed more massive than a turnoff star and are formed by the merger of two or more parent MS stars. In particular, Shara et al. (1997) and Sepinsky et al. (2000) have directly measured the masses of several blue stragglers in the cores of 47 Tuc and NGC 6397 and confirmed that they are well above the MS turnoff mass, some even with masses apparently above *twice* the turnoff mass. Furthermore, Gilliland et al. (1998) have demonstrated that the masses estimated from the pulsation frequencies of four oscillating blue stragglers in 47 Tuc are consistent with their positions in the CMD.

Stellar mergers can occur through either a direct collision or the coalescence of a binary system (Leonard 1989; Livio 1993; Stryker 1993; Bailyn 1995). Single-single star collisions occur with appreciable frequency only in the cores of the densest clusters (Hills & Day 1976),

but in lower-density clusters collisions can also happen indirectly, during resonant interactions involving binaries (Leonard 1989; Leonard & Fahlman 1991; Sigurdsson et al. 1994; Sigurdsson & Phinney 1995; Davies & Benz 1995; Bacon et al. 1996). Merger rates depend directly on cluster properties such as the local density, velocity dispersion, mass function, and binary fraction. When mergers do occur, all of these cluster properties are affected. The dynamics of a cluster, including mass segregation and the rate of core collapse, are consequently influenced, leading to an intricate relation between individual stellar interactions and cluster evolution (Elson et al. 1987; Rasio 2000). By studying stellar mergers, we are therefore able to probe the dynamics of globular clusters. Results from ongoing *Hubble Space Telescope* surveys of nearby globular clusters continue to expand the statistics of blue straggler populations, making it timely for a detailed comparison between observations and theory.

The final structure and chemical composition profiles of merger remnants are of central importance, since they determine the subsequent observable properties and evolutionary tracks of merger products in a CMD (Sills & Bailyn 1999). Three-dimensional hydrodynamic simulations is one means by which we can focus on fluid mixing during stellar mergers and determine the structure of a remnant. Many such simulations of stellar mergers have been presented in the literature (Lombardi et al. 1996; Sandquist et al. 1997; Sills & Lombardi 1997; Sills et al. 2001). The problem with these simulations, if they were to be coupled with calculations of the cluster as a whole, is the prohibitive computing time: high resolution hydrodynamic simulations can typically take hundreds or even thousands of hours to complete.

In this paper, we develop a method for computing the structure and composition profiles of zero-age blue stragglers *without* running hydrodynamic simulations. Since our method takes considerably less than a minute to generate a model on a typical workstation, we are able to explore the results of collisions in a drastically shorter amount of time. Our approach can be generalized to work for more than two parent stars, simply by colliding two stars first and then colliding the remnant with a third parent star. Most importantly, such algorithms will make it possible to incorporate the effects of collisions in simulations of globular clusters as a whole.

2. Procedure

We begin with two (non-rotating) parent star models, specifying initial profiles for the stellar density ρ, pressure P, and abundance of chemicals as a function of mass fraction. The profile for the entropic variable $A \equiv P/\rho^{\Gamma}$, a quantity closely related (but not equal) to

thermodynamic entropy, can also be calculated easily and is of central importance. Here Γ is the adiabatic index of the gas. Since the quantity A depends directly upon the chemical composition and the entropy, it remains constant for each fluid element in the absence of shocks.

Fluid elements with low values of A sink to the bottom of a gravitational potential well, and the A profile of a star in stable dynamical equilibrium increases radially outwards. Indeed, it is straightforward to show that the condition $\mathrm{d}A/\mathrm{d}r > 0$ is equivalent to the usual Ledoux criterion for convective stability of a nonrotating star (Lombardi et al. 1996). The basic idea here can be seen by considering a small fluid element inside a non-rotating star in dynamical equilibrium. If this element is perturbed outward adiabatically (that is, with constant A), then it it will sink back towards equilibrium only if its new density is larger than that of its new environment. If instead the element is less dense than its surroundings, it will continue to float away from the equilibrium, an unstable situation. Likewise, if an element is perturbed inward, its density needs to be less than the environment's in order to return towards equilibrium. Since pressure equilibrium between the element and its immediate environment is established nearly instantaneously, the ratio of densities satisfies $\rho_{\mathrm{element}}/\rho_{\mathrm{environment}} = (A_{\mathrm{element}}/A_{\mathrm{environment}})^{-1/\Gamma}$, by the definition of A. Therefore if the perturbed element has a larger A than its new environment, then it has a lower density and buoyancy will push the element outwards. Similarly, a fluid element with a lower A then its surroundings will sink. As a result, a stable stratification of fluid requires that the entropic variable A increase outward: $\mathrm{d}A/\mathrm{d}r > 0$. In such a star, a perturbed element will experience restoring forces that cause it to oscillate about its equilibrium position. For a detailed discussion of the stability conditions within rotating stars, see §7.3 of Tassoul (1978) or Tassoul (2000). In practice, even in rapidly rotating stars, fluid distributes itself in such a way that the entropic variable A increases outwards.

During a collision, the entropy A of a fluid element can increase due to shock heating (see §2.2). However, the relative impact speed of two MS stars in a globular cluster is comparable to the speed of sound in these parents: both of these speeds are of order $(GM/R)^{1/2}$, where G is Newton's gravitational constant, and M and R are respectively the mass and length scales of a parent star. Consequently, the resulting shocks have Mach numbers of order unity and shock heating is relatively weak. Therefore, to a reasonable approximation, a fluid element maintains a constant A throughout a collision.

The underlying principle behind our method exploits the two special properties of A that were just discussed. Namely, the entropic variable A will (1) increase outward in a stable star and (2) be nearly conserved during a collision. Therefore, to a good approximation, *the distribution of fluid in a collisional remnant can be determined simply by sorting the fluid*

from both parent stars in order of increasing A: the lowest A fluid from the parent stars is placed at the core of the remnant and is surrounded by shells with increasingly higher A. In this paper, we will further improve upon this approximation by also modeling mass loss, shock heating, fluid mixing, and the angular momentum distribution.

Our algorithms are calibrated from the results of smoothed particle hydrodynamic (SPH) calculations presented in Lombardi et al. (1996) (for collisions of polytropic stars) as well as in Sills & Lombardi (1997) and Sills et al. (2001) (for collisions of more realistically modeled stars). For reviews of SPH, see Monaghan (1992) or Rasio & Lombardi (1999). For details and tests of our SPH code, see Lombardi et al. (1999).

2.1. Mass Loss

The velocity dispersion of globular cluster stars is typically only ~ 10 km s^{-1}, which is much smaller than the escape velocity from the surface of a MS star; for example, a star of mass $M = 0.8M_\odot$ and radius $R = R_\odot$ has an escape velocity $(2GM/R)^{1/2} = 552$ km s^{-1}. For this reason, collisional trajectories are well approximated as parabolic, and the mergers are relatively gentle: the mass lost is never more than about 8% of the total mass in the system (mass loss with hyperbolic trajectories is treated by Lai, Rasio & Shapiro (1994)). Furthermore, most main sequence stars in globular clusters are not rapidly rotating, and it is a good approximation to treat the initial parent stars as non-rotating.

Given models for the parent stars (see Table 1), we first determine the mass lost during a collision. Inspection of hydrodynamic results for collisions between realistically modeled stars, as well as for collisions between polytropes, suggests that the fraction of mass ejected can be estimated approximately by

$$f_L = c_1 \frac{\mu}{M_1 + M_2} \frac{R_{1,0.9} + R_{2,0.9}}{R_{1,0.7} + R_{2,0.7} + c_2 r_p}, \tag{1}$$

where c_1 and c_2 are dimensionless constants that we take to be $c_1 = 0.21$ and $c_2 = 3$, $\mu \equiv M_1 M_2/(M_1 + M_2)$ is the reduced mass of the parent stars, $R_{i,0.7}$ and $R_{i,0.9}$ are the radii in parent star i enclosing a mass fraction $m/M_i = 0.7$ and 0.9, respectively, and r_p is the periastron separation for the initial parabolic orbit. While developing equation (1) we searched for a relation that accounted for the *mass distribution* (not just the total masses and radii) of the parent stars in some simple way. The more diffuse the outer layers of the parents, the longer the stellar cores are able to accelerate towards each other after the initial impact: the $R_{1,0.7} + R_{2,0.7}$ in the denominator of equation (1) accounts for this increased effective collision speed for parents whose mass distributions are more centrally concentrated. The

dependence on μ in equation (1) arises from the expectation that the mass loss will be roughly proportional to the kinetic energy at impact, and from the fact that a simple rescaling of the stellar masses ($M_i \rightarrow kM_i$) in a hydrodynamic simulation leaves f_L unchanged. This method yields remnant masses that are seldom more than $\sim 0.01 M_\odot$ different than what is given by a hydrodynamic simulation (see the last two columns of Table 2); this is clearly a significant improvement over neglecting mass loss completely, which sometimes can overestimate the remnant mass by more than $\sim 0.1 M_\odot$.

The final (post-shock) value of a fluid element's entropic variable will be slightly larger than its initial value, as discussed in §2.2. The mass loss must be distributed between the two parent stars such that the outermost fluid layers retained from each parent has the same final entropic variable A, so that the layers can merge together into a stable equilibrium. We solve for this maximum value of A in the remnant by requiring that the mass of the fluid with larger final A be the desired ejecta mass.

2.2. Shock Heating

Shocks increase the value of a fluid element's entropic variable $A = P/\rho^\Gamma$. The distribution and timing of shock heating during a collision involve numerous complicated processes: each impact generates a recoil shock at the interface between the stars, the oscillating merger remnant sends out waves of shock rings, and finally the outer layers of the remnant are shocked as gravitationally bound ejecta fall back to the remnant surface. For off-axis collisions this may be repeated several times. Our goal is not to *derive* approximations describing the shock heating during each of these stages, but rather empirically to determine physically reasonable relations that fit the available SPH data.

Let A and A_{init} be, respectively, the final and initial values of the entropic variable for some particular fluid element. We used the results of hydrodynamic calculations to examine how the change $A - A_{init}$, as well as the ratio A/A_{init}, depended on a variety of functions of P_{init} (the initial pressure) and A_{init}. Our search for a simple means of modeling this dependence was guided by a handful of features evident from hydrodynamic simulations: (1) fluid deep within the parents are shielded from the brunt of the shocks, (2) in head-on collisions, fluid from the less massive parent experiences less shock heating than fluid with the same initial pressure from the more massive parent, (3) in off-axis collisions with multiple periastron passages before merger, fluid from the less massive parent experiences more shock heating than fluid with the same initial pressure from the more massive parent, and (4) the shock heating within each parent clearly must be the same if the two parent stars are identical. In all of the hydrodynamic calculations considered we model the fluid

in our system using an adiabatic index $\Gamma = 5/3$, corresponding to an ideal gas equation of state.

We find that when $\log_{10}(A - A_{init})$ is plotted versus $\log_{10}(P_{init})$, the resulting curve for each parent star is fairly linear (see Fig. 1) with a slope of approximately $c_3 = -1.1$ throughout most of the remnant in the ~ 25 simulations we examined:

$$\log_{10}(A - A_{init}) = b_i(r_p) - c_3 \log_{10} P_{init}, \quad i = 1, 2. \tag{2}$$

Here the intercept $b_i(r_p)$ is a function of the periastron separation r_p for the initial parabolic trajectory as well as the masses M_1 and M_2 of the parent stars. Larger values of b_i correspond to larger amounts of shock heating in star i, where the index $i = 1$ for the more massive parent and $i = 2$ for the less massive parent ($M_2 < M_1$). For simplicity of notation, we have suppressed the index i on the A, A_{init} and P_{init} in equation (2).

The SPH data suggest that the intercepts $b_i(r_p)$ can be fit according to the relations

$$b_1(r_p) = b_1(0) - c_4 \frac{r_p}{R_1 + R_2} \log_{10}(M_1/M_2) \tag{3}$$

$$b_2(r_p) = b_1(0) + \left(c_5 \frac{r_p}{R_1 + R_2} - c_6 \right) \log_{10}(M_1/M_2), \tag{4}$$

where $c_4 = c_5 = 7$, $c_6 = 2.6$, and $b_1(0)$ is the intercept for a head-on collision ($r_p = 0$) between the two parent stars under consideration. Our method for determining $b_1(0)$ is discussed below. Clearly, expressions such as equations (2), (3) and (4) are rather crude approximations that lump together complicated effects from the various stages of the fluid dynamics. However, these expressions do work surprisingly well when M_1 and M_2 are at least roughly comparable in magnitude. Furthermore, this treatment does necessarily imply the desirable qualitative features discussed above: (1) fluid with large initial pressure P_{init} (the fluid shielded by the outer layers of the star) is shock heated less, (2) $b_2(0) < b_1(0)$, so that the smaller star is shock heated less in head-on collisions, (3) $b_1(r_p)$ increases with r_p while $b_2(r_p)$ decreases with r_p, so that for sufficiently large r_p we have $b_2(r_p) > b_1(r_p)$ and the less massive star is shock heated more, and (4) $b_1(r_p) = b_2(r_p)$ whenever $M_1 = M_2$, so that identical parent stars always experience the same level of shock heating.

Although equations (2), (3) and (4) describe how to distribute the shock heating, the overall strength of the shock heating hinges on the value chosen for $b_1(0)$. To determine $b_1(0)$, we consider the head-on collision between the parent stars under consideration and exploit conservation of energy: more specifically, we choose the value of $b_1(0)$ that ensures that the initial energy of the system equals the final energy during a head-on collision. Since we are considering parabolic collisions, the orbital energy is zero and the initial energy is simply $E_{tot} = E_1 + E_2$, the sum of the energies for each of the parent stars. The final energy

of the system includes energy associated with the ejecta and the center of mass motion of the remnant, in addition to the energy E_r of the remnant in its own center of mass frame. In this paper we consider non-rotating parent stars, and so the remnant of a headon collision also is non-rotating and its structure quickly approaches spherically symmetry. The values of E_1, E_2 and E_r are therefore simply the sum of the internal and self-gravitational energies calculated while integrating the equation of hydrostatic equilibrium. Since the energy E_r depends on the thermodynamic profiles of the remnant, it is therefore a function of a shock heating parameter $b_1(0)$ (see §2.3 for the details of how the remnant's structure is determined).

The energy E_r of the remnant is nearly equal to the initial energy E_{tot} of the system. However, the ejecta do carry away a portion of the total energy, suggesting that the energy conservation equation be written as

$$E_{tot} = E_r - c_7 f_L E_{tot}, \tag{5}$$

where the coefficient c_7 is order unity and f_L is the fraction of mass lost during the collision (see §2.1). We use a value of $c_7 = 2.5$, which is consistent with all the available SPH data. In equation (5), the left hand side is the initial energy of the system, and the right hand side is its final energy. The second term on the right hand side accounts for the energy associated with the ejecta and with any center of mass motion of the remnant (note that this term is positive since $E_{tot} < 0$). In practice, we iterate over $b_1(0)$ until equation (5) is solved. Equation (5) needs to be solved only once for each pair of parent star masses M_1 and M_2: once $b_1(0)$ is known, we can model shock heating in a collision with any periastron separation r_p by first calculating $b_1(r_p)$ and $b_2(r_p)$ from equations (3) and (4) and by then using these values in equation (2).

2.3. Merging and Fluid Mixing

As with any star in stable dynamical equilibrium, the remnant will have an A profile that increases outward. In our model, fluid elements with a particular A value in both parent stars will mix to become fluid in the remnant with the same value of the entropic variable. Furthermore, if the fluid in the core of one parent star has a lower A value than any of the fluid in the other parent star, the former's core must become the core of the remnant, since the latter cannot contribute at such low entropies. When merging the fluid in the two parent stars to form the remnant, we use the post shock entropic variable A, as determined from equation (2).

Within the merger remnant, the mass m_r enclosed within a surface of constant A must

equal the sum of the corresponding enclosed masses in the parents:

$$m_r|_{A_r=A} = m_1|_{A_1=A} + m_2|_{A_2=A}\,. \tag{6}$$

It immediately follows that the derivative of the mass in the remnant with respect to A equals the sum of the corresponding derivatives in the parents: $\mathrm{d}m_r/\mathrm{d}A_r = \mathrm{d}m_1/\mathrm{d}A_1 + \mathrm{d}m_2/\mathrm{d}A_2$, or $dA_r/dm_r = [(dA_1/dm_1)^{-1} + (dA_2/dm_2)^{-1}]^{-1}$. We calculate these derivatives using simple finite differencing. Consequently, if we break our parent stars and merger remnant into mass shells, then two adjacent shells in the remnant that have enclosed masses that differ by Δm_r will have entropic variables that differ by

$$\Delta A_r = \frac{\Delta m_r}{\left(\frac{dA_1}{dm_1}\right)^{-1} + \left(\frac{dA_2}{dm_2}\right)^{-1}}. \tag{7}$$

The value of A at a particular mass shell in the remnant is then determined by adding ΔA_r to the value of A in the previous mass shell.

In the case of the (non-rotating) remnants formed in head-on collisions, knowledge of the A profile is sufficient to determine uniquely the pressure P, density ρ, and radius r profiles. While forcing the A profile to remain as was determined from sorting the shocked fluid, we integrate numerically the equation of hydrostatic equilibrium with $\mathrm{d}m = 4\pi r^2 \rho \mathrm{d}r$ to determine the ρ and P profiles [which are related through $\rho = (A/P)^{3/5}$]. This integration is an iterative process, as we must initially guess at the central pressure. Our boundary condition is that the pressure must be zero when the enclosed mass equals the desired remnant mass $M_r = (1 - f_L)(M_1 + M_2)$. During this numerical integration we also determine the remnant's total energy E_r and check that the virial theorem is satisfied to high accuracy. The total remnant energy E_r appears in equation (5), and if this equation is not satisfied to the desired level of accuracy, we adjust our value of $b_1(0)$ accordingly and redo the shocking and merging process.

As done in Sills et al. (2001), the structure of a rotating remnant can be determined by integrating modified equations of equilibrium (see eq. (9) of Endal & Sofia (1976)), once the entropy A and specific angular momentum j distribution are known (see §2.4). To do so, one can implement an iterative procedure in which initial guesses at the central pressure and angular velocity are refined until a self-consistent model is converged upon. Even for the case of off-axis collisions and rotating remnants, the chemical composition profiles can still be determined, even without solving for the pressure and density profiles, as we will now discuss.

Once the A profile of the remnant has been determined, we focus our attention on its chemical abundance profiles. Not all fluid with same initial value of A_{init} is shock heated

by the same amount during a collision, since, for example, fluid on the leading edge of a parent star is typically heated more violently than fluid on the trailing edge of the parent. Consequently, fluid from a range of initial shells in the parents can contribute to a single shell in the remnant. To model this effect, we first mix each parent star by spreading out its chemicals over neighboring mass shells, using a Gaussian-like distribution that depends on the difference in enclosed mass between shells. Let X_i be the chemical mass fraction of some species X in a particular shell i, and let the superscripts "pre" and "post" indicate pre- and post-mixing values, respectively. Then

$$X_k^{post} = \sum_i \frac{X_i^{pre} g_{ik} \Delta m_i}{\sum_j g_{ji} \Delta m_j}, \tag{8}$$

$$g_{ik} = \exp\left[-\frac{\alpha}{M^2}(m_i - m_k)^2\right] + \exp\left[-\frac{\alpha}{M^2}(m_i + m_k)^2\right] + \exp\left[-\frac{\alpha}{M^2}(m_i + m_k - 2M)^2\right], \tag{9}$$

$$\alpha = c_8 \left(M \overline{\frac{d \ln A}{dm}}\right)^2, \tag{10}$$

where Δm_i is the mass of shell i, m_i is the mass enclosed by shell i, M is the total mass of the parent star, and c_8 is a dimensionless coefficient that we choose to be $c_8 = 1.5$. We have suppressed an additional index in equations (8) through (10) that would label the parent star. The summand in equation (8) is the contribution from shell i to shell k. The second term in the distribution function, equation (9), is important only for mass shells near the center of the parent, while the third term becomes important only for mass shells near the surface; these two correction terms guarantee that an initially chemically homogeneous star remains chemically homogeneous during this mixing process ($X_k^{post} = X_k^{pre}$ =constant, for any shell k). The bar in equation (10) represents an average over the parent star, and the dependence of α on the average $d \ln A/dm$ ensures that stars with steep entropy gradients are more difficult to mix [see Table 4 of Lombardi et al. (1996)].

Consider a fluid layer of mass dm_r in the merger remnant with an entropic variable A that ranges from A_r to $A_r + dA_r$. The fraction of that fluid dm_i/dm_r that originated in parent star i can be calculated as $(dA_r/dm_r)/(dA_i/dm_i)$. Therefore, the composition of this fluid element can be determined by the weighted average

$$X_r = X^{post,1} \frac{dA_r/dm_r}{dA_1/dm_1} + X^{post,2} \frac{dA_r/dm_r}{dA_2/dm_2}, \tag{11}$$

where all derivatives are evaluated at A_r, the value of the entropic variable under consideration. Equation (11) allows us to determine the final composition profile of any merger remnant simply from the A profiles of the parent stars and merger remnant, as well as the (post-mixed) composition profile of each parent as given by equation (8).

2.4. Angular Momentum Distribution

To estimate the total angular momentum J_r of the remnant in its center of mass frame, we use angular momentum conservation in the same way that energy conservation was used in §2.2. In particular, since the parent stars are non-rotating, the total angular momentum in the system is just the orbital angular momentum,

$$J_{tot} = M_1 M_2 \left(\frac{2Gr_p}{M_1 + M_2} \right)^{1/2}, \tag{12}$$

which we set equal to J_r plus a contribution due to mass loss [cf. eq. (5)]:

$$J_{tot} = J_r + c_9 f_L J_{tot}. \tag{13}$$

The SPH simulations demonstrate that J_{tot} is always slightly larger than J_r, and the choice $c_9 = 2.2$ leads to good agreement with the SPH results. Equation (13) can be solved for J_r, and the results are compared with those of SPH simulations for a few typical cases in Table 3. The agreement (between the numbers in the last two columns) is excellent.

The structure of the rotating remnants formed in off-axis collisions depends on the distribution of this specific angular momentum within the remnant. Even though the collisional remnants are axisymmetric around the rotation axis with angular velocities Ω that are constant on isodensity surfaces, the specific angular momentum distribution can nevertheless be quite complicated [see Fig. 12 of Lombardi et al. (1996) or Fig. 3 of Sills et al. (2001)]. The goal here is to simplify this complicated distribution into an average one-dimensional profile. The specific angular momentum j for the SPH remnants increases outward and is typically concave upward throughout most of the remnant when averaged over isodensity surfaces and plotted against enclosed mass.

Once an approximate analytic *form* for the average j profile (which is only weakly dependent on the periastron separation r_p) is specified, the profile can be normalized simply by requiring

$$J_r = \int_0^{M_r} j(m) dm, \tag{14}$$

where m corresponds to the mass enclosed within a constant density surface and J_r is determined from equation (13). We find that, unlike a simple power-law dependence, the approximate relation $j(m) \propto \left[(m/M_r)^{-2/3} - c_{10} \right]^{-1}$ (with $c_{10} = 0.8$) is able to reproduce the qualitative features of the angular momentum profile. Using equation (14) to find the proportionality coefficient, one obtains

$$j(m) = \frac{c_{10}^{5/2}}{3 \tanh^{-1}(c_{10}^{1/2}) - 3c_{10}^{1/2} - c_{10}^{3/2}} \frac{J_r}{M_r} \left[\left(\frac{m}{M_r} \right)^{-2/3} - c_{10} \right]^{-1}. \tag{15}$$

Other forms for $j(m)$ could also be used, being normalized through equation (14). One advantage of equation (15) is that for $m << M_r$ the specific angular momentum $j(m)$ scales like $m^{2/3}$, in agreement with both simple analytic treatments and SPH results.

3. Results

3.1. Comparison with Three-Dimensional Hydrodynamic Models

To test the accuracy of our simple models, we compare their structure and composition against models generated directly from the results of SPH calculations. These SPH calculations include both collisions between polytropic parent models (referred to with a capital letter as the case name) and collisions between realistically modeled parent stars (referred to with a lower case letter). Characteristics of the various parent stars used are summarized in Table 1, while the various collision scenarios we have considered are listed, along with mass loss information, in Table 2.

The realistically modeled parent stars are based on calculations done with the Yale Rotating Evolution Code (YREC), as discussed in Sills & Lombardi (1997). In particular, we evolved non-rotating main-sequence stars with a primordial helium abundance $Y = 0.25$ and metallicity $Z = 0.001$ for 15 Gyr, the amount of time needed to exhaust the hydrogen in the center of the $0.8 M_\odot$ star. The thermodynamic profiles of these parent stars are shown in Figure 2. We note that $P/\rho^{5/3}$ decreases slightly in the outermost layers of the $0.4 M_\odot$ and $0.6 M_\odot$ stars. The adiabatic index Γ is actually less than the ideal gas value of 5/3 in these regions, due to the relative importance of ionization and radiation pressure. In this paper, however, we neglect these effects and instead simply force the A profile to increase by some negligibly small amount in these regions. Figure 3 displays the chemical abundance profiles of these parent stars.

The first collision studied in Sills & Lombardi (1997), Case a, is between two (turnoff) $0.8\,M_\odot$ stars, and the second, Case g, is between a $0.8 M_\odot$ star and a $0.4 M_\odot$ star. The total energy of the system in Case a is $E_{tot} = -5.23 \times 10^{48}$ erg, and consequently, using the treatment outlined in this paper, we find that the total energy of the remnant is $E_r = -6.29 \times 10^{48}$ erg [see eq. (5)]. For Case g, these energies are -3.35×10^{48} erg and -3.90×10^{48} erg. Furthermore, $\alpha = 309$ for the parents in Case a, while for Case g, $\alpha_1 = 308$ for the $0.8 M_\odot$ parent and $\alpha_2 = 91$ for the $0.4 M_\odot$ parent.

Thermodynamic (Fig. 4) and chemical composition (Figs. 5, 6, 7 and 8) profiles show that our remnant models are quite accurate. In Case g, our remnant displays the kink in the A profile near $m/M = 0.1$ (see Fig. 4), inside of which the fluid originates solely from

the $0.8M_{\odot}$ star. Our models also reproduce the chemical profiles of the SPH remnant very well: the peak values in the chemical abundances are often accurate to within 10%, and the shapes of these profiles, though sometimes peculiar, are followed closely. Helium distribution is particularly important to model well since it will determine the MS lifetime of the remnant. The central values of the fractional helium abundance Y given by our model differ from the SPH result by only about 5% or less.

It is interesting to note that there is very little lithium in our remnants. Lithium is burned during stellar evolution except at low temperatures, and therefore can be used as an indicator of mixing. If a star has a deep enough surface convective layer, there will be essentially no lithium, because the convection mixes any lithium from the outer layers into the hot interior where it is burned. A small amount of lithium in our $0.8M_{\odot}$ parent star does exist in the outer few percent of its mass (see Fig. 3) and consequently becomes part of the ejecta during the collision. Although near the remnant's surface our method yields a large *fractional* error in lithium abundance (see Figs. 5 and 6), this is simply because the overall abundance is so close to zero. For example, the predicted surface fractional Li^6 abundance of 4.6×10^{-11} for our Case a remnant is an overestimate, but is more than 20 times smaller than the surface fractional abundance in the $0.8M_{\odot}$ parent. Except for in the extreme case of grazing collisions (when mass loss is exceedingly small), collisional blue stragglers should be severely depleted in lithium, a prediction that can be tested with appropriate observations [see Shetrone & Sandquist (2000) and Ryan et al. (2001)].

In addition to the chemical distribution in our rotating remnants, good agreement between our simple models and their corresponding SPH counterparts is also found in the angular momentum distribution. Specific angular momentum profiles, averaged over surfaces of constant density, are compared in Figure 9 for Cases e, f and k. Note that the hump in the SPH j profile in the outer few percent of the remnant is due to having to terminate the simulation before all of the gravitationally bound fluid has fallen back to the merger remnants: this feature is still diminishing gradually during the final stage of the SPH calculation and hence we do not attempt to model it.

3.2. Stellar Evolution of Remnant Models

A rigorous test of the validity of the simple models, which we have performed using YREC, is to compare their subsequent stellar evolution against that of SPH-generated models. YREC evolves a star through a sequence of models of increasing age, solving the linearized stellar evolution equations for interior profiles such as chemical composition, pressure, temperature, density and luminosity. All relevant nuclear reactions (including pp-chains, the

CNO cycle, triple-α reactions and light element reactions) are treated. Recent opacity tables are used (ensuring that the remnant's position in a CMD can be accurately determined) and mixing mechanisms are incorporated. For blue stragglers, the various mixing processes can potentially carry fresh hydrogen fuel into the stellar core and thereby extend the MS lifetime of the remnant. Furthermore, any helium mixed into the outer layers affect the opacity and hence the remnant's position in a CMD. The free parameters in YREC (e.g., the mixing length) are set by calibrating a solar mass and solar metallicity model to the Sun.

Using the method described in Sills et al. (1997), we used two of our simple models (Cases a and g) as starting models in YREC and evolved the collision products from the end of the collision to the giant branch. Figure 10 shows the evolutionary tracks for these simple models (solid lines) and the SPH-generated models (dotted lines). The tracks of the SPH-generated models are discussed in Sills & Lombardi (1997).

The agreement between the two sets of models is very good. Although there are some differences on the 'pre-main sequence' portion of the tracks, this represents only a very small fraction of the total lifetime of the collision products. In both cases, the SPH models begin their evolution at higher luminosities than the simple models. Once the collision product reaches the main sequence, the two methods show very good agreement, and the subgiant and giant branch evolution of these stars is virtually identical. The main sequence lifetimes for the two different methods agree reasonably well. For Case g, the SPH results give a lifetime of 850 Myr, while the simple models give 720 Myr. For Case a, the SPH results give a lifetime of 80 Myr, compared to 150 Myr from the simple models. The larger relative difference for Case a is largely determined by the lower central helium abundance Y of the simple models. While these lifetimes differ by nearly a factor of two, the lifetime of Case a is a very small fraction of the lifetime of globular clusters, and therefore the simple models can still be useful for incorporating stellar collisions into dynamical models of globular cluster evolution.

The algorithms we have developed are implemented in a FORTRAN software package that can be downloaded from http://vassun.vassar.edu/∼lombardi/mmas/. This software could be used in combination with realistic dynamical simulations of star clusters that must take into account stellar collisions.

We thank J. Faber for his contributions to the SPH code, and A. Thrall for testing our software package and for helpful comments. J.C.L. acknowledges support from the Keck Northeast Astronomy Consortium, from a grant from the Research Corporation, and from NSF Grant AST-0071165. F.A.R. acknowledges support from NSF Grants AST-9618116 and PHY-0070918, NASA ATP Grant NAG5-8460, and a Sloan Research Fellowship. This

work was also partially supported by the National Computational Science Alliance under Grant AST980014N and utilized the NCSA SGI/Cray Origin2000 parallel supercomputer.

REFERENCES

Bacon, D., Sigurdsson, S., & Davies, M. B. 1996, MNRAS, 281, 830

Bailyn, C. D. 1995, Ann. Rev. Ast. Astrop., 33, 133

Davies, M. B., & Benz, W. 1995, MNRAS, 276, 876

Elson, E., Hut, P., & Inagaki, S. 1987, Ann. Rev. Astr. Ap. 25, 565

Endal, A. S., & Sofia, S. 1976, ApJ, 210, 184

Gilliland, R. L. 1998, ApJ, 507, 818

Hills, J. G., & Day, C. A. 1976, Ap. Letters, 17, 87

Lai, D. Rasio, F. A. & Shapiro, S. L. 1994, ApJ, 423, 344.

Leonard, P. J. T. 1989, AJ, 98, 217

Leonard, P. J. T., & Fahlman, G. G. 1991, AJ, 102, 994

Livio, M. 1993, in *Blue Stragglers*, ASP Conf. Ser. 53, ed. R. A. Saffer (San Francisco: ASP)

Lombardi, J. C., Jr., Rasio, F. A., & Shapiro, S. L. 1996, ApJ, 468, 797

Monaghan, J. J. 1992, ARA&A, 30, 543

Lombardi, J. C., Sills, A., Rasio, F. A., & Shapiro, S. L. 1999, J. Comp. Phys., 152, 687

Rasio, F. A., & Lombardi, J. C. 1999, J. Comp. App. Math., 109, 213

Rasio, F. A. 2000, to appear in Dynamics of Star Clusters and the Milky Way, eds. S. Deiters et al. (ASP Conference Series) [astro-ph/0006205]

Ryan, S., Beers, T., Kajino, T. & Rosolankova, K. 2001, ApJ, 547, 231

Sandquist, E. L., Bolte, M. & Hernquist, L. 1997, ApJ, 477, 335

Sepinsky, J. F., Saffer, R. A., Pilman, C. S., DeMarchi,G., & Paresce, F. 2000, AAS Meeting 196, #41.06

Shara, M. M., Saffer, R. A., & Livio, N. 1997, ApJ, 489, L59

Shetrone, M.D., & Sandquist, E.L. 2000, AJ, 120, 1913

Sigurdsson, S., Davies, M. B., & Bolte, M. 1994, ApJ, 431, L115

Sigurdsson, S., & Phinney, E. S. 1995, ApJS, 99, 609

Sills, A., & Bailyn, C. D. 1999, ApJ, 513, 428

Sills, A. & Lombardi, J. C. 1997, ApJ, 487, 290

Sills, A., Lombardi, J. C., Jr., Demarque, P. D., Bailyn, C. D., Rasio, F. A., & Shapiro, S. L. 1997, ApJ, 487, 290

Sills, A., Bailyn, C. D., Edmonds, P. D., & Gilliland, R. L. 2000, ApJ, 535, 298

Sills, A., Faber, J. A., Lombardi, J. C., Rasio, F. A., & Warren, A. R. 2001, ApJ, 548, 323

Stryker, L. L. 1993, PASP, 105, 1081

Tassoul, J. 1978, Theory of Rotating Stars (Princeton: Princeton Univ. Press)

Tassoul, J. 2000, Stellar Rotation (Cambridge: Cambridge Univ. Press)

AAS LaTeX macros v5.0.

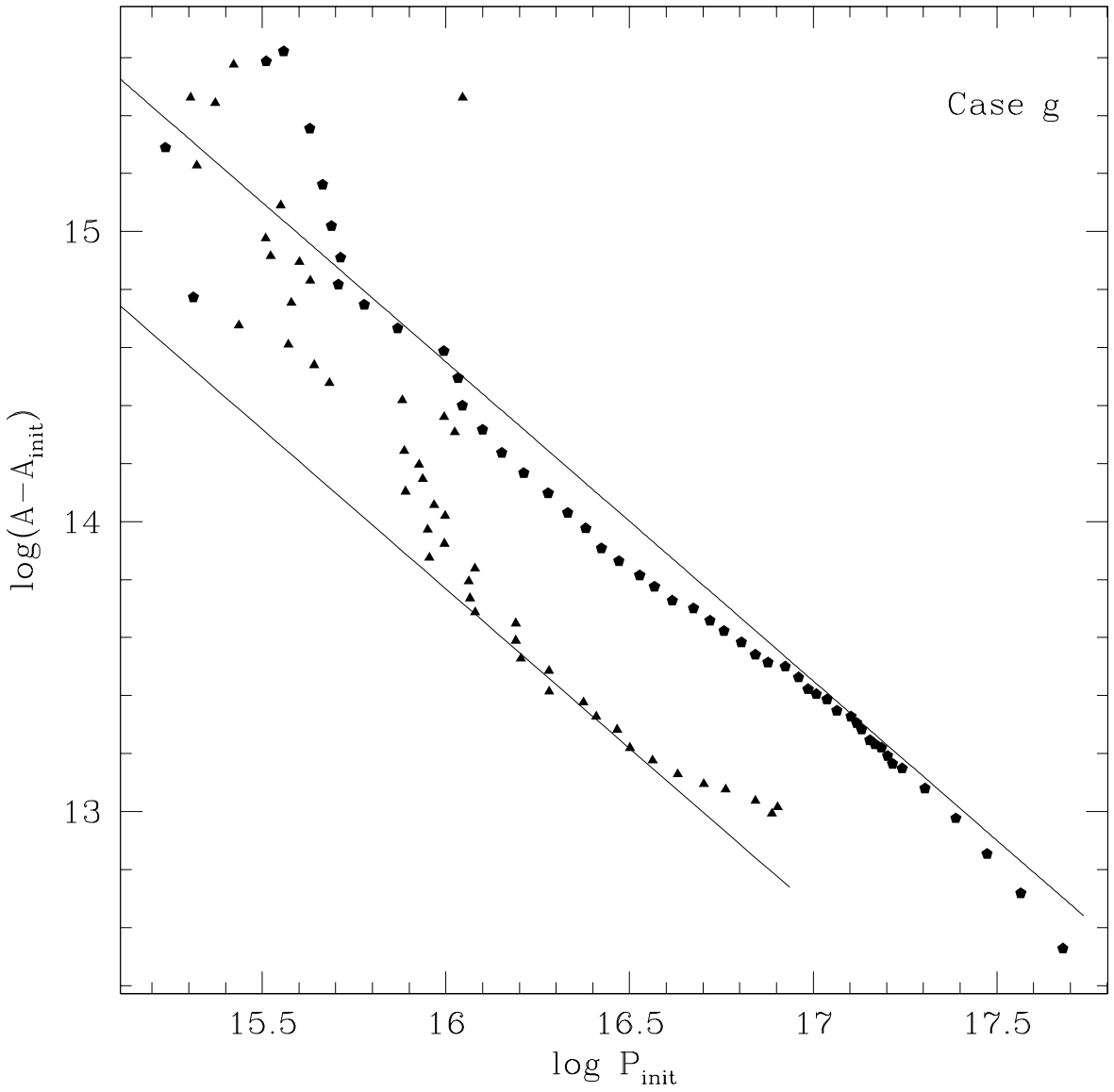

Fig. 1.— The change in entropic variable A as a function of initial pressure P_{init} on a log plot for the SPH remnant in Case g (head-on collision of $M_1 = 0.8M_\odot$ and $M_2 = 0.4M_\odot$ realistically modelled parent stars). Pentagons refer to fluid from parent star 1 that has reached dynamical equilibrium by the end of the simulation and that has be binned by enclosed mass fraction; triangles refer to the corresponding fluid from star 2. The lines are fits to the data with slopes of -1.1 and intercepts b_i that differ by $2.6 \log_{10}(M_1/M_2)$ [see eqs. (2) – (4)]. Logarithms are base 10 and units are cgs.

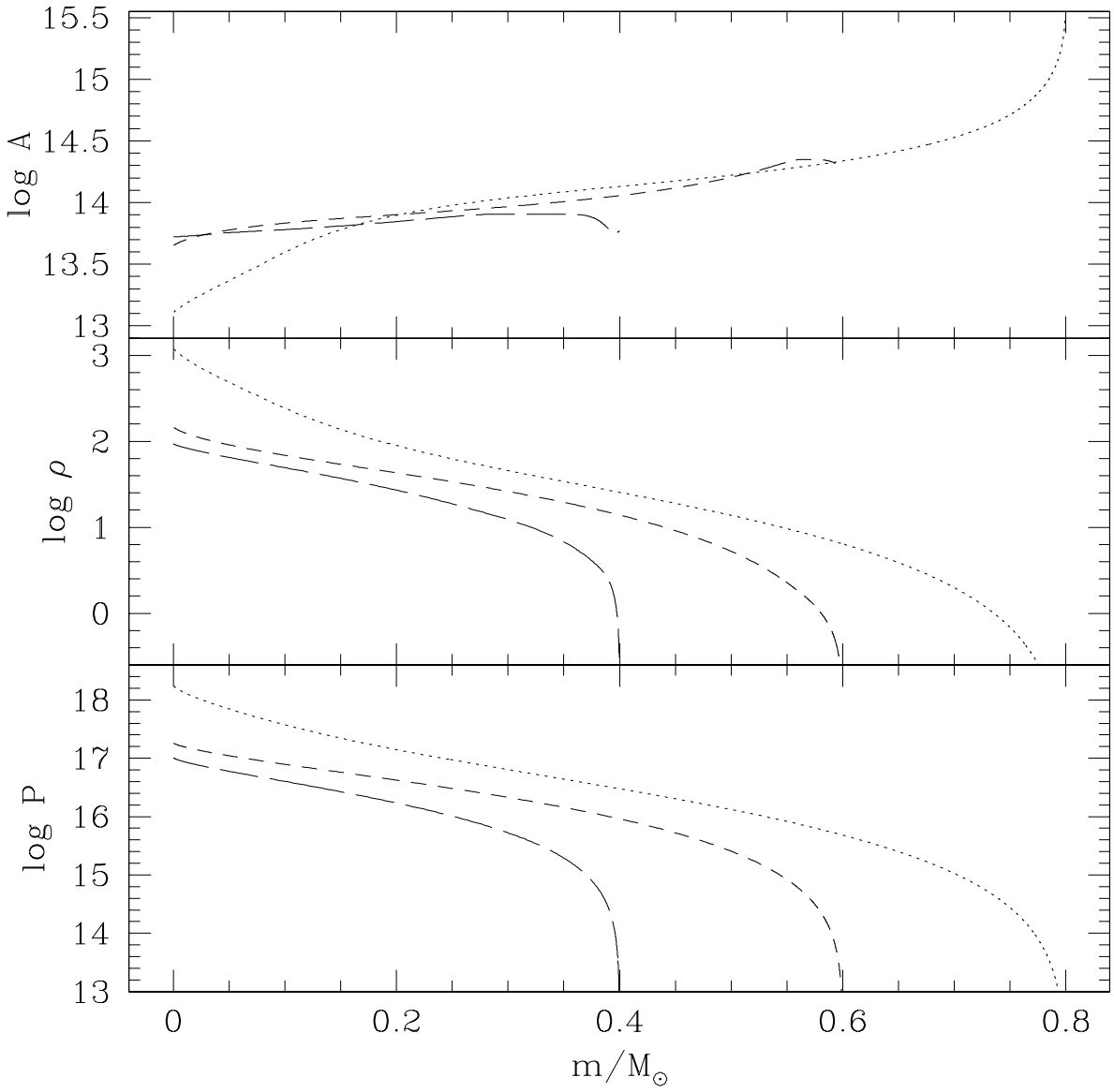

Fig. 2.— Thermodynamic profiles of $A(= P/\rho^{5/3})$, pressure P, and density ρ as a function of enclosed mass m for three realistically modeled parent stars. The long-dashed, short-dashed and dotted curves refer to a $0.4M_\odot$, $0.6M_\odot$ and $0.8M_\odot$ parent star, respectively. Logarithms are base 10 and units are cgs.

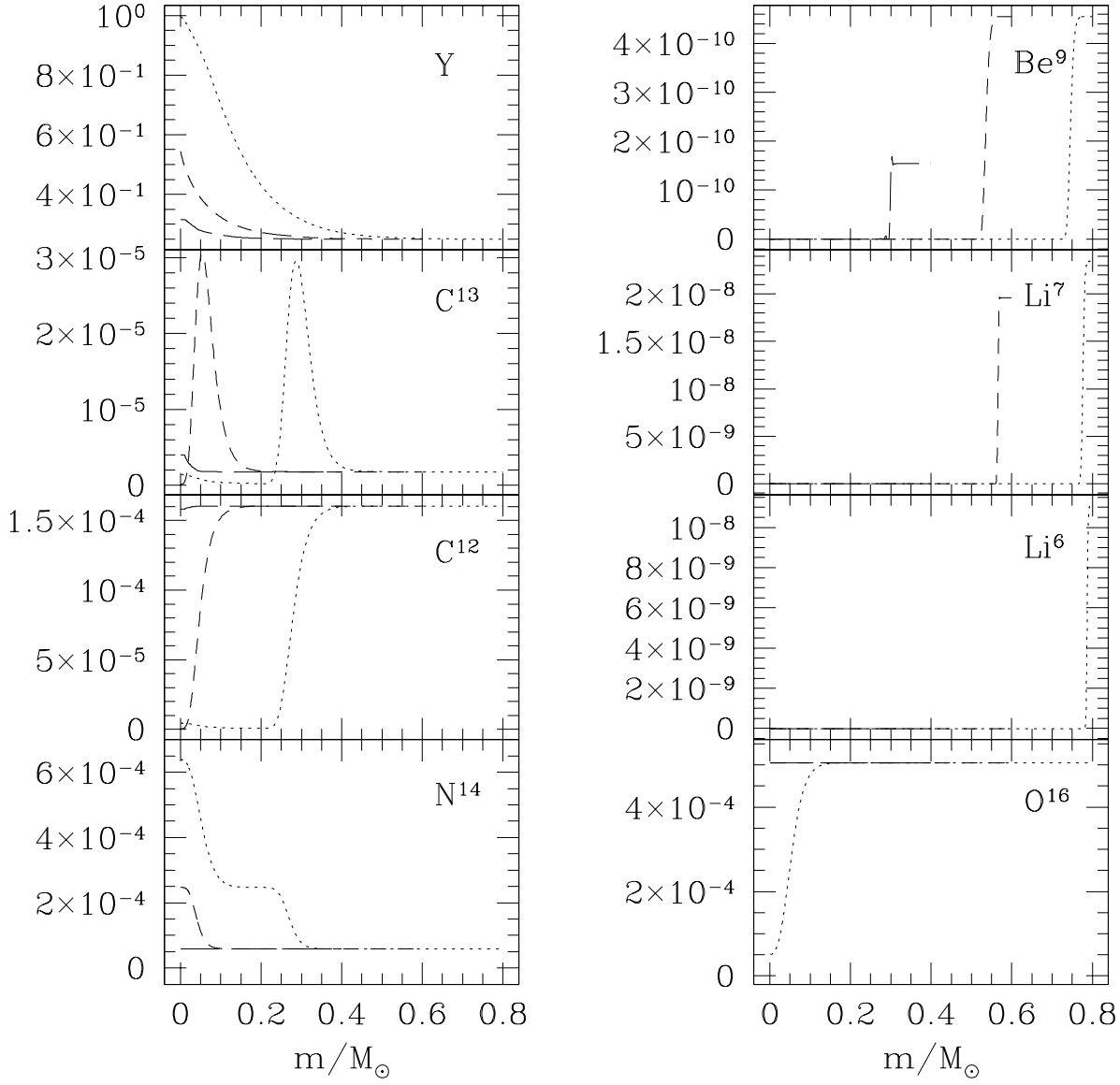

Fig. 3.— Fractional chemical abundance (by mass) as a function of enclosed mass m for various chemical elements in our three parent stars. Line types are as in Fig. 2.

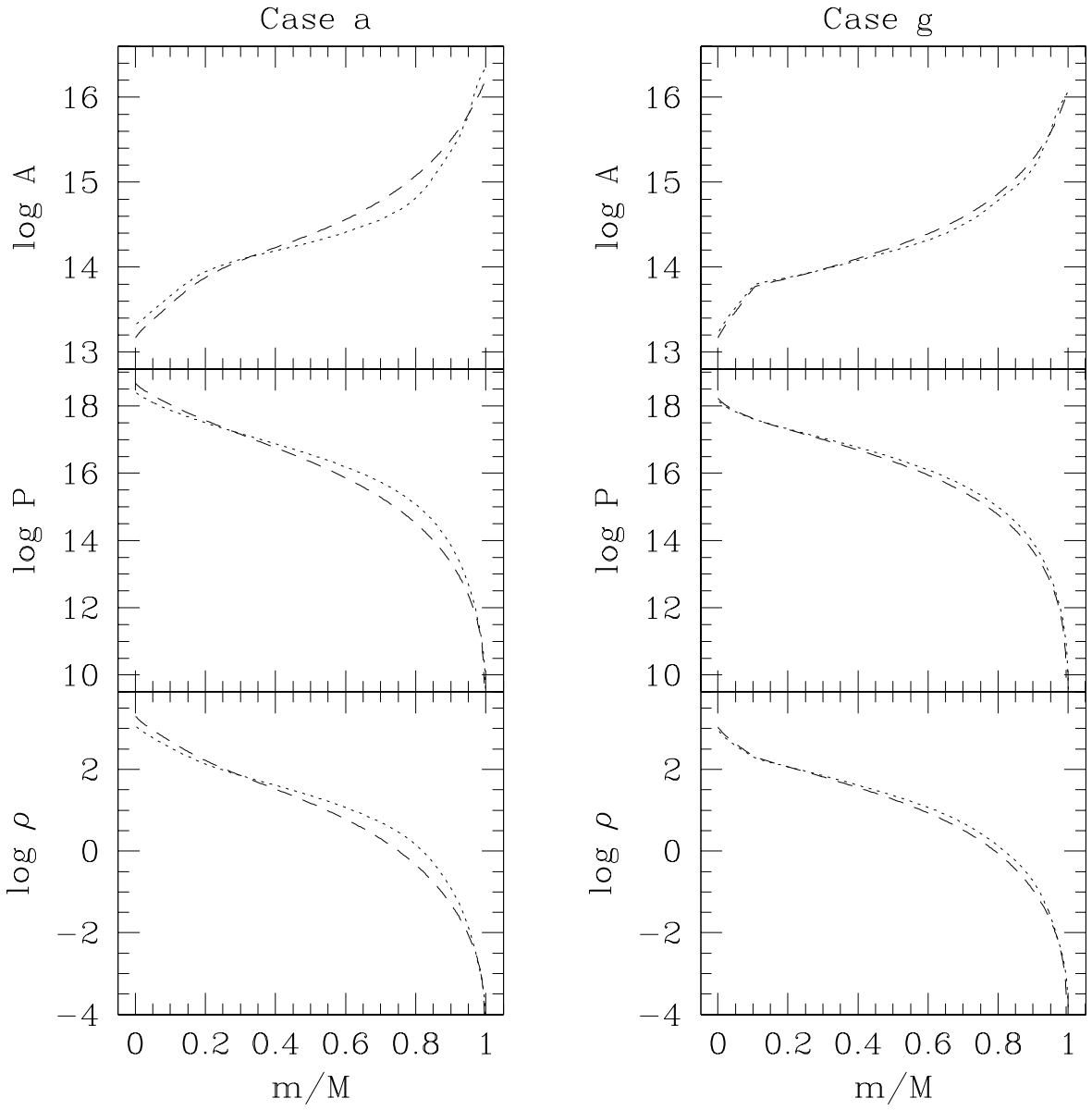

Fig. 4.— Thermodynamic profiles of A, pressure P, and density ρ as a function of enclosed mass fraction m/M for the remnants of Cases a and g, where M is the total bound mass of the remnant. The dotted line refers to the remnant resulting from a 3D SPH simulation, and the dashed line refers to the remnant generated by the method of this paper. Logarithms are base 10 and units are cgs.

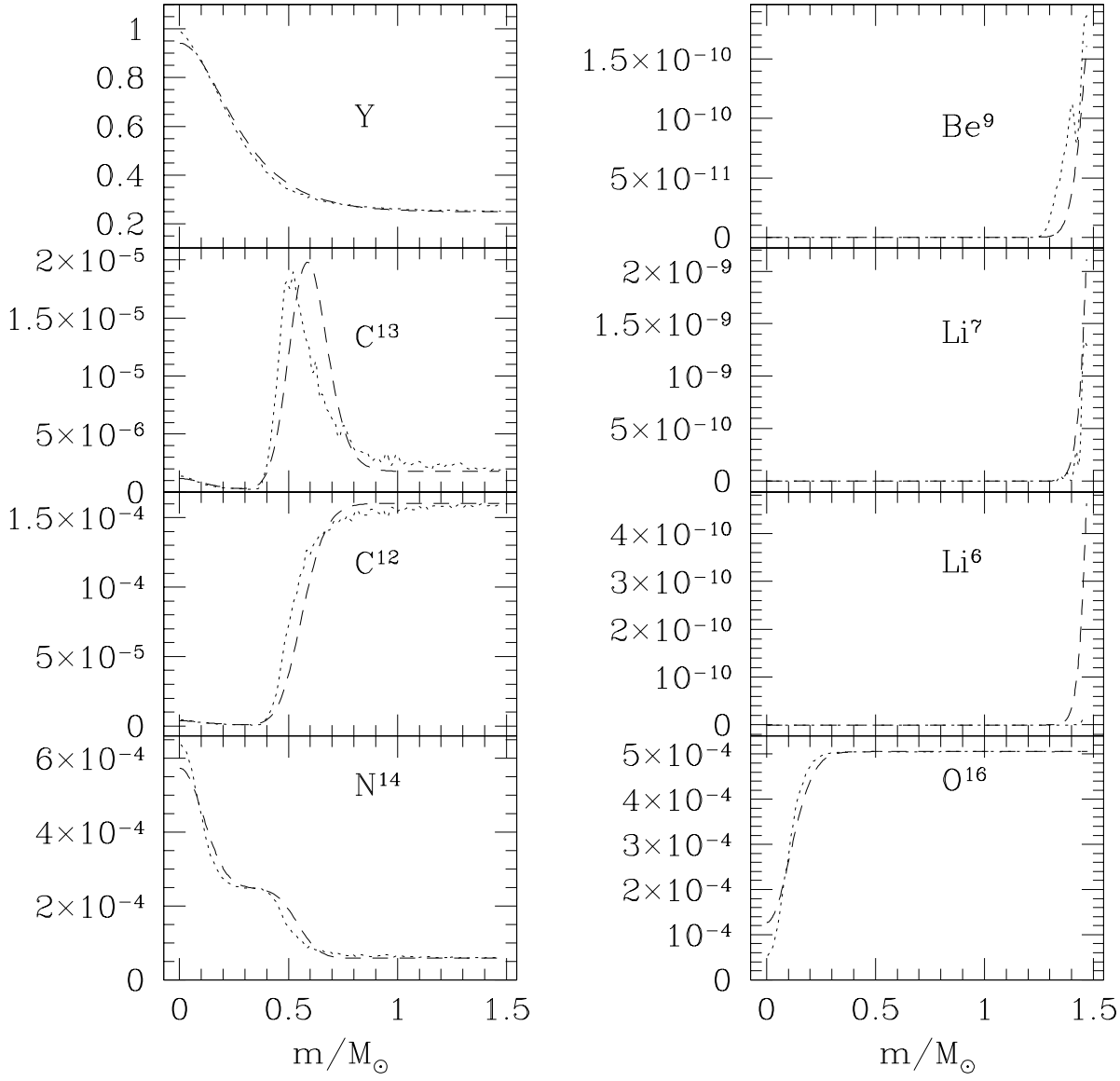

Fig. 5.— Fractional chemical abundance (by mass) as a function of enclosed mass fraction m/M for the Case a remnant. Line types are as in Fig. 4.

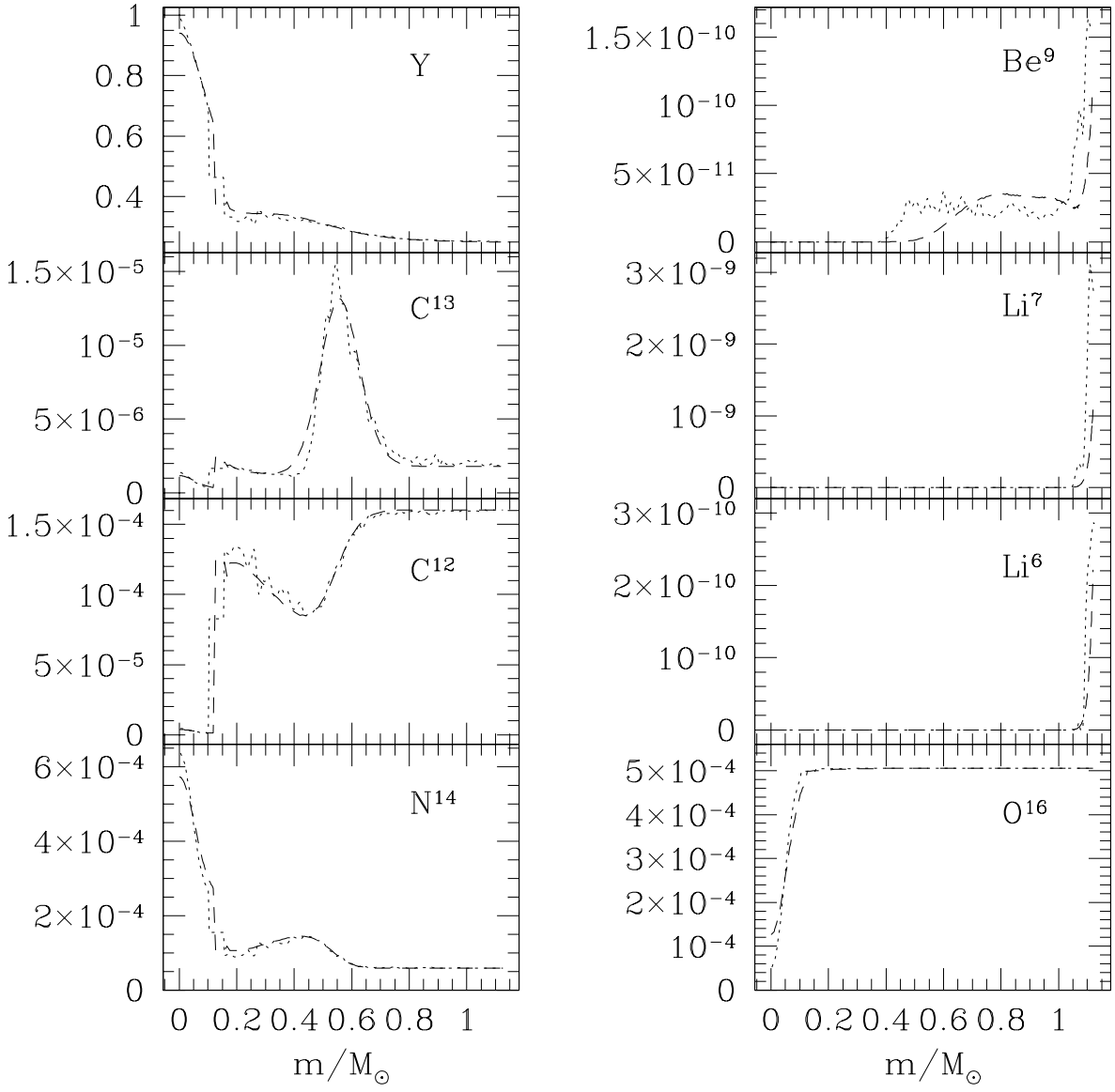

Fig. 6.— Fractional chemical abundance (by mass) as a function of enclosed mass fraction m/M for the Case g remnant. Line types are as in Fig. 4.

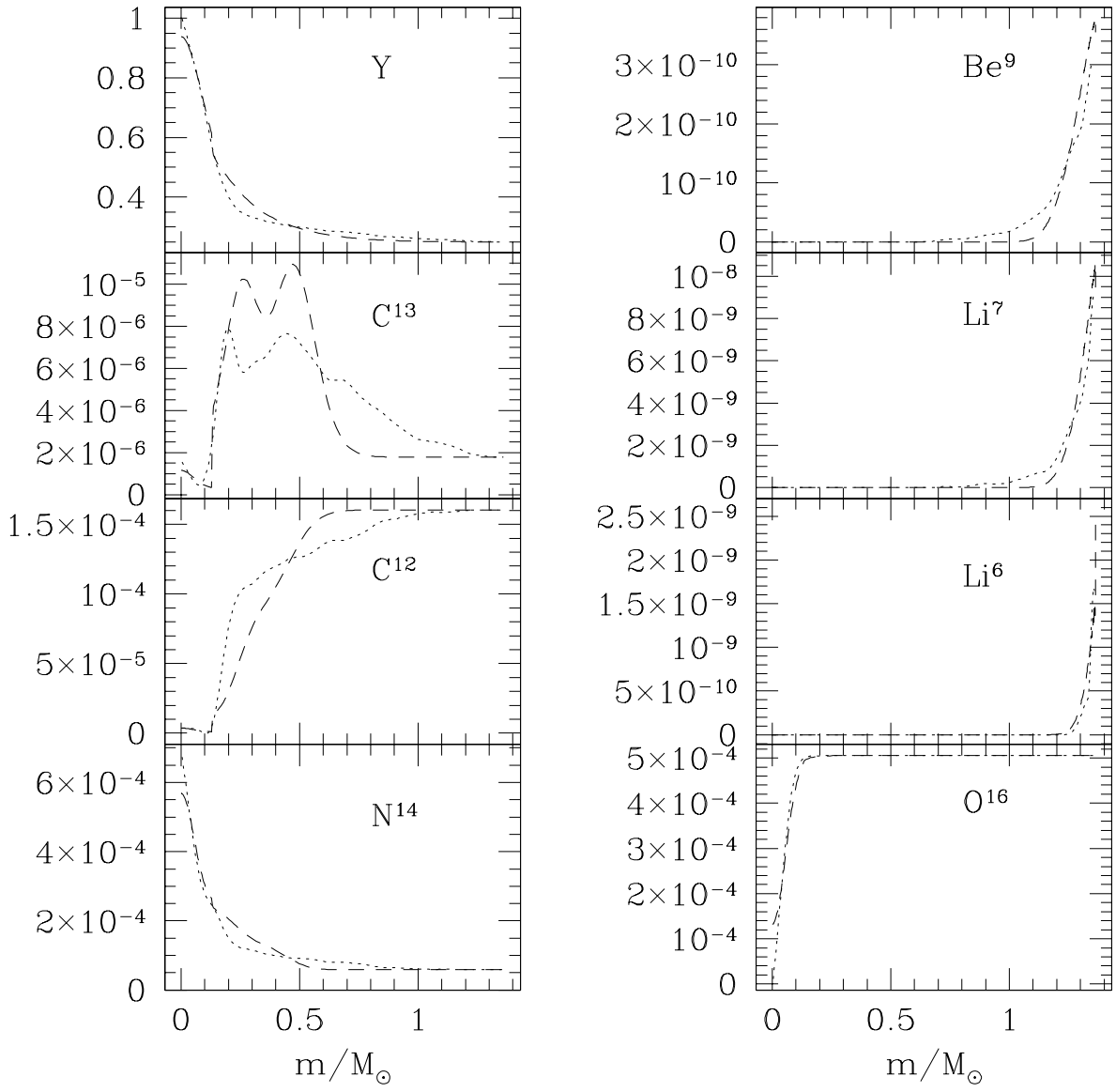

Fig. 7.— Fractional chemical abundance (by mass) as a function of enclosed mass fraction m/M for the Case e remnant. Line types are as in Fig. 4.

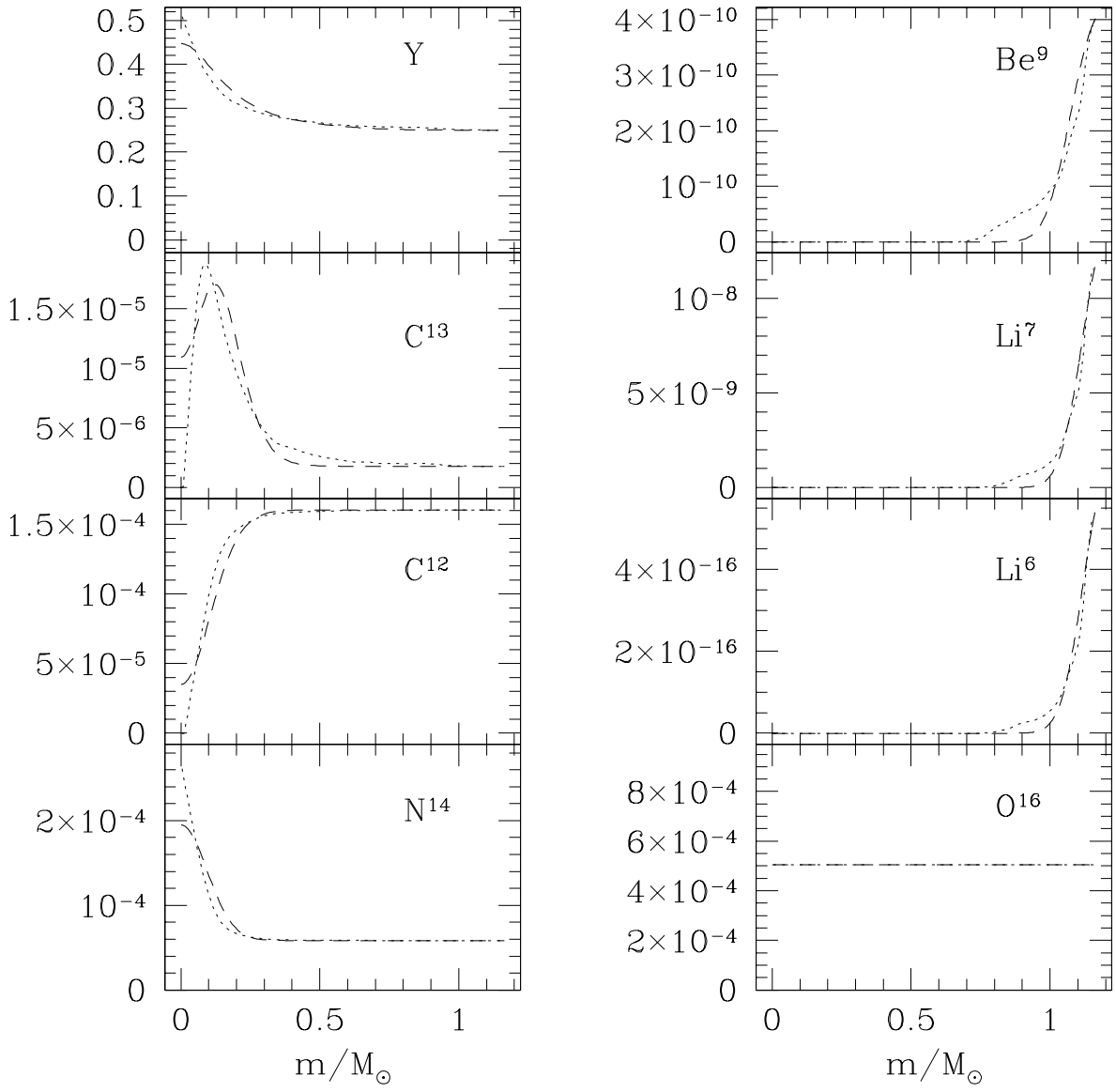

Fig. 8.— Fractional chemical abundance (by mass) as a function of enclosed mass fraction m/M for the Case k remnant. Line types are as in Fig. 4.

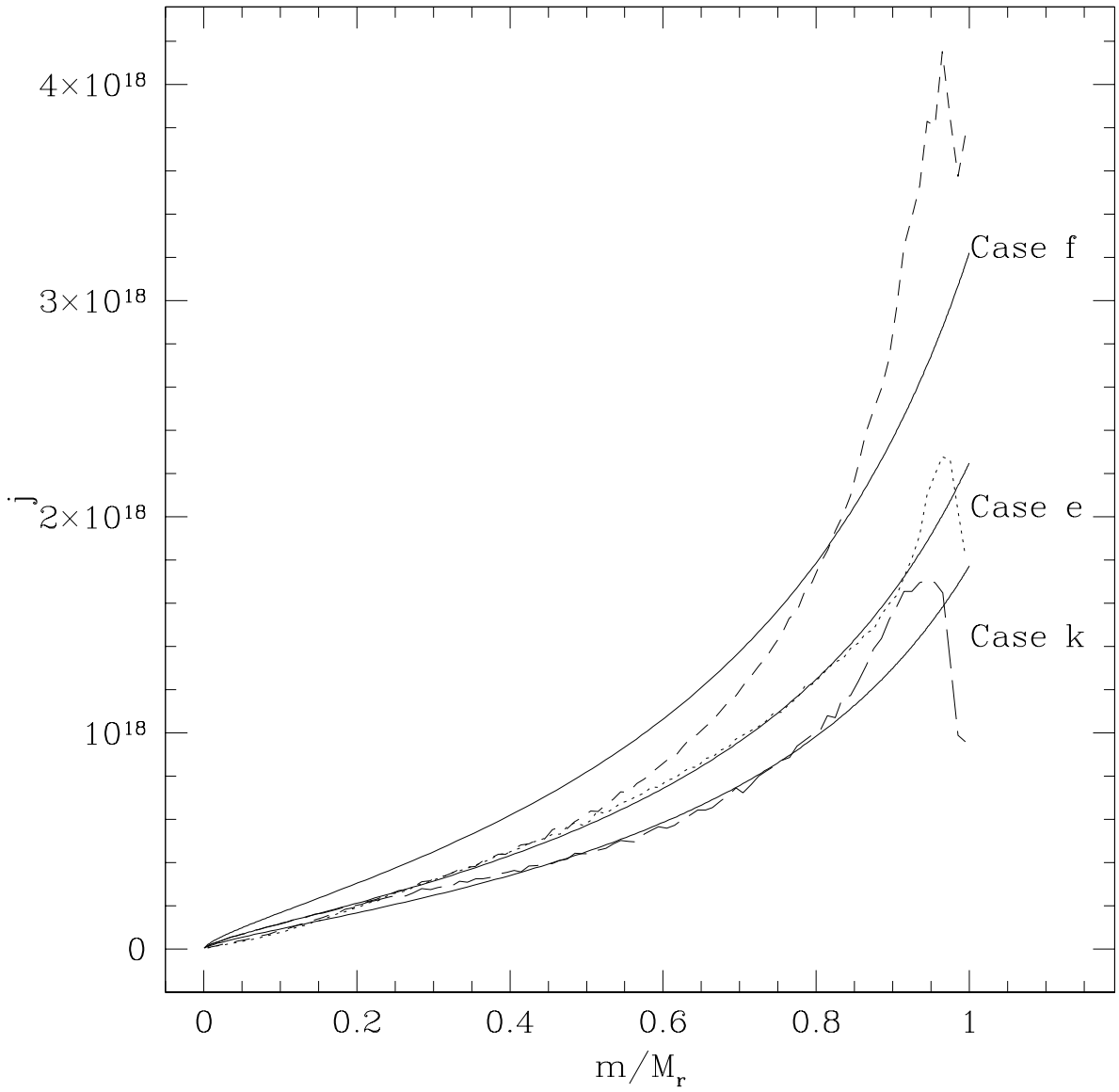

Fig. 9.— SPH specific angular momentum profiles compared with the approximate profiles (solid curves) generated from equation (15). Note that the hump in the SPH j profile in the outer few percent of the remnant results from the need to terminate the simulation before all of the gravitationally bound fluid has fallen back to the merger remnants. Units are cgs.

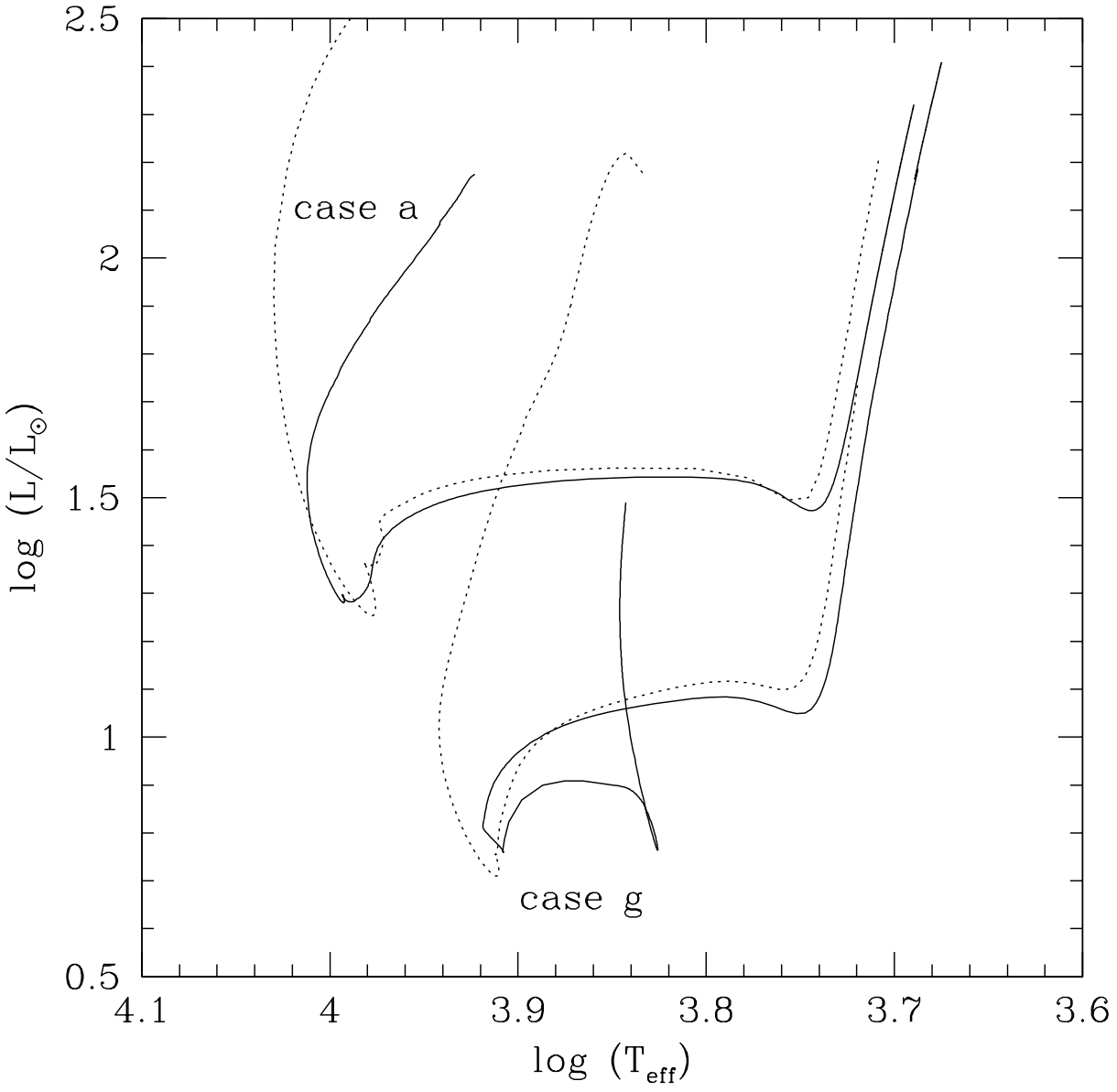

Fig. 10.— Evolutionary tracks for Case a and Case g. The solid lines correspond to the tracks of the simple models described in this paper. The dotted lines show tracks for which the starting model was generated from the output of SPH simulations of stellar collisions.

Table 1. Parent Star Characteristics

Model type	$M[M_\odot]$	$R[R_\odot]$	$R_{0.7}[R_\odot]$	$R_{0.9}[R_\odot]$
Polytropic	0.8	0.955	0.38	0.48
Polytropic	0.6	0.54	0.36	0.40
Polytropic	0.4	0.35	0.25	0.27
Polytropic	0.16	0.15	0.11	0.12
Realistic	0.8	0.955	0.284	0.442
Realistic	0.6	0.517	0.262	0.360
Realistic	0.4	0.357	0.227	0.287

Table 2. Mass loss

Case[a]	$M_1[M_\odot]$	$M_2[M_\odot]$	$r_p/(R_1+R_2)$	$f_{L,SPH}$[b]	f_L[c]	$M_{SPH}[M_\odot]$[d]	$M_r[M_\odot]$[e]
A	0.8	0.8	0.00	0.064	0.066	1.50	1.494
B	0.8	0.8	0.25	0.023	0.023	1.56	1.563
C	0.8	0.8	0.50	0.012	0.014	1.58	1.578
D	0.8	0.6	0.00	0.057	0.067	1.32	1.306
E	0.8	0.6	0.25	0.024	0.025	1.37	1.365
F	0.8	0.6	0.50	0.008	0.015	1.39	1.379
G	0.8	0.4	0.00	0.056	0.056	1.13	1.133
H	0.8	0.4	0.25	0.028	0.022	1.17	1.174
I	0.8	0.4	0.50	0.008	0.014	1.19	1.184
J	0.6	0.6	0.00	0.049	0.059	1.14	1.129
K	0.6	0.6	0.25	0.028	0.028	1.17	1.167
L	0.6	0.6	0.50	0.022	0.018	1.17	1.178
M	0.6	0.4	0.00	0.054	0.056	0.95	0.944
N	0.6	0.4	0.25	0.029	0.027	0.97	0.973
O	0.6	0.4	0.50	0.010	0.018	0.99	0.982
P	0.4	0.4	0.00	0.037	0.057	0.77	0.754
Q	0.4	0.4	0.25	0.029	0.028	0.78	0.778
R	0.4	0.4	0.50	0.010	0.018	0.79	0.785
S	0.4	0.4	0.75	0.008	0.014	0.79	0.789
T	0.4	0.4	0.95	0.011	0.011	0.79	0.791
U	0.8	0.16	0.00	0.026	0.036	0.94	0.926
V	0.8	0.16	0.25	0.025	0.013	0.94	0.947
W	0.8	0.16	0.50	0.021	0.008	0.94	0.952
a	0.8	0.8	0.00	0.080	0.082	1.47	1.469
e	0.8	0.6	0.25	0.029	0.025	1.36	1.365
f	0.8	0.6	0.50	0.014	0.015	1.38	1.379
g	0.8	0.4	0.00	0.063	0.067	1.12	1.120
k	0.6	0.6	0.25	0.032	0.029	1.16	1.165

[a]Capital letters refer to collisions of polytropic stars (Lombardi et al. 1996); lower case letters refer to cases involving more realistically modeled parent stars (Sills & Lombardi 1997; Sills et al. 2001)

[b]The fractional mass loss as determined by an SPH simulation

[c]The fractional mass loss as estimated by equation (1)

[d]The remnant mass as determined by an SPH simulation

[e]The remnant mass as estimated by $(1 - f_L)(M_1 + M_2)$

Table 3. Total Angular Momentum

Case	J_{tot}[a] [g cm^2/s]	$J_{r,SPH}$[b] [g cm^2/s]	J_r[c] [g cm^2/s]
E	2.12×10^{51}	2.04×10^{51}	2.00×10^{51}
I	2.02×10^{51}	1.97×10^{51}	1.96×10^{51}
e	2.10×10^{51}	1.99×10^{51}	1.99×10^{51}
f	2.97×10^{51}	2.85×10^{51}	2.87×10^{51}
k	1.43×10^{51}	1.36×10^{51}	1.34×10^{51}

[a]The total angular momentum in the system's center of mass frame.

[b]The angular momentum of the remnant in its center of mass frame, as determined by an SPH simulation

[c]The angular momentum of the remnant in its center of mass frame, as determined by eq. (13)